

Supplementary Materials for

Recording interfacial currents on the subnanometer length and femtosecond time scale by terahertz emission

Eric Yue Ma, Burak Guzel Turk, Guoqing Li, Linyou Cao, Zhi-Xun Shen, Aaron M. Lindenberg, Tony F. Heinz*

*Corresponding author. Email: tony.heinz@stanford.edu

Published 8 February 2019, *Sci. Adv.* **5**, eaau0073 (2019)
DOI: 10.1126/sciadv.aau0073

This PDF file includes:

- Fig. S1. Schematic of the time-domain TES setup.
- Fig. S2. Reproducibility of the measurements.
- Fig. S3. Comparison between the low- and high-bandwidth data.
- Fig. S4. Typical reflectance contrast and Raman spectra of the heterostructures.
- Fig. S5. Analysis of the optical properties calculation.
- Fig. S6. Determination of THz refractive index of GaP.
- Fig. S7. Total transfer function of the setup.
- Fig. S8. Normalized THz waveforms for representative excitation fluences.
- Fig. S9. Reflected excitation power as a function of excitation fluence.

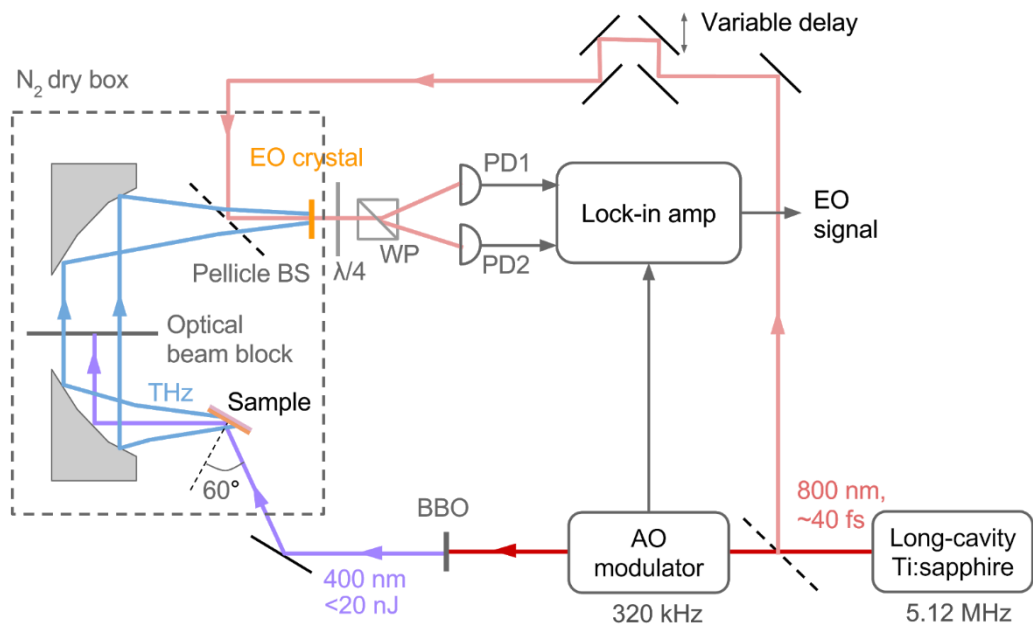


Fig. S1. Schematic of the time-domain TES setup. AO is acousto-optic, BS beamsplitter, WP Wollaston prism, and PD1&2 the balanced photodetectors. The optical beam block is a 500- μm -thick high-resistivity Si wafer. The EO crystal is either a 1-mm-thick ZnTe or a 258- μm -thick GaP. We use a N_2 dry box to eliminate absorption by water vapor in air.

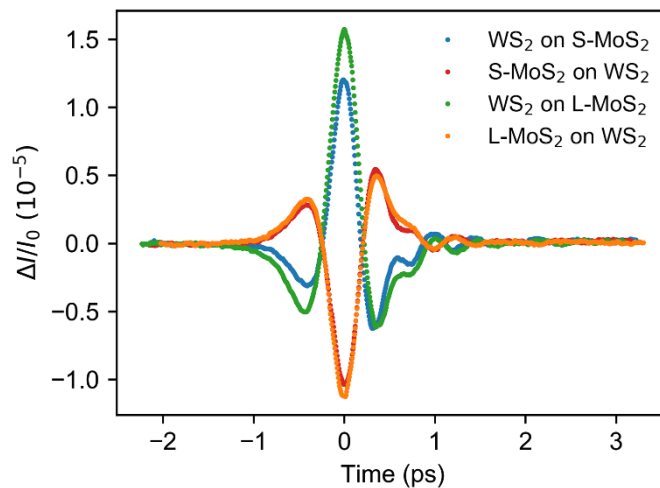


Fig. S2. Reproducibility of the measurements. EO sampling data for heterostructures made with small (S-) and large grain (L-) MoS_2 monolayers. The sign reversal is not affected by the material quality and the field strengths are within 10-20%.

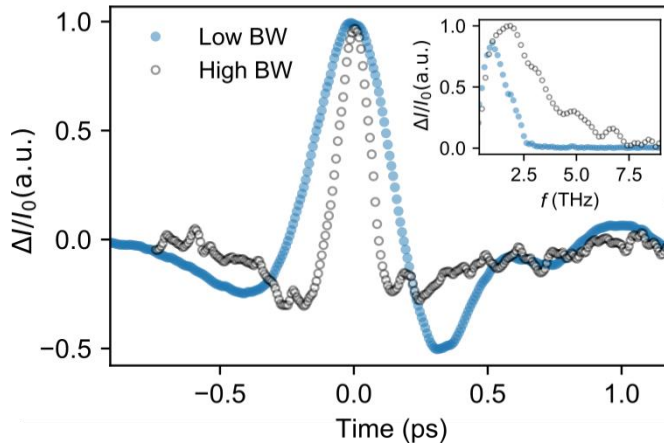


Fig. S3. Comparison between the low- and high-bandwidth data (from Fig. 1 and 3, respectively) for the same WS₂ on MoS₂ heterostructure in time and frequency (inset) domain. The low- and high-bandwidth data were taken with 1 mm BBO/1 mm ZnTe and 200 μm BBO/258 μm GaP as crystals for generation of 3.1 eV excitation pulses and for detection of the THz electric field.

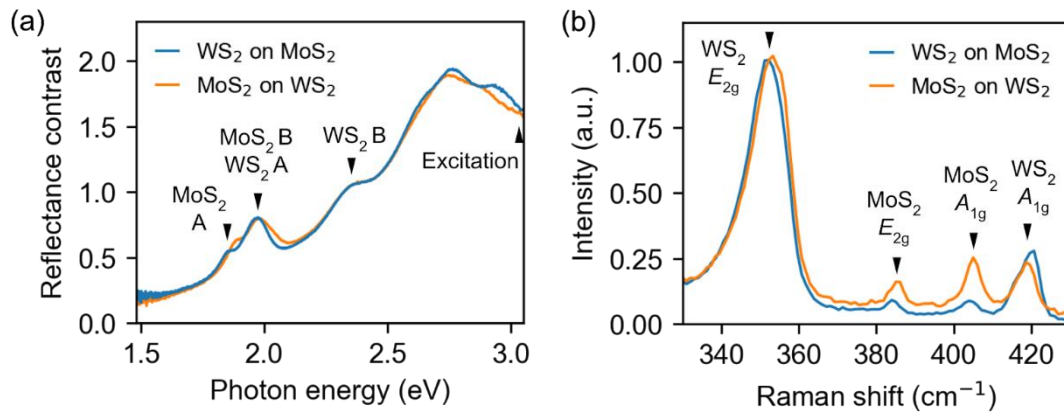


Fig. S4. Typical reflectance contrast and Raman spectra of the heterostructures. Typical reflectance contrast spectra identifying the positions of the A and B excitons of MoS₂ and WS₂ (a) and Raman spectra identifying the E_{2g} and A_{1g} phonon modes (b) of the heterostructures.

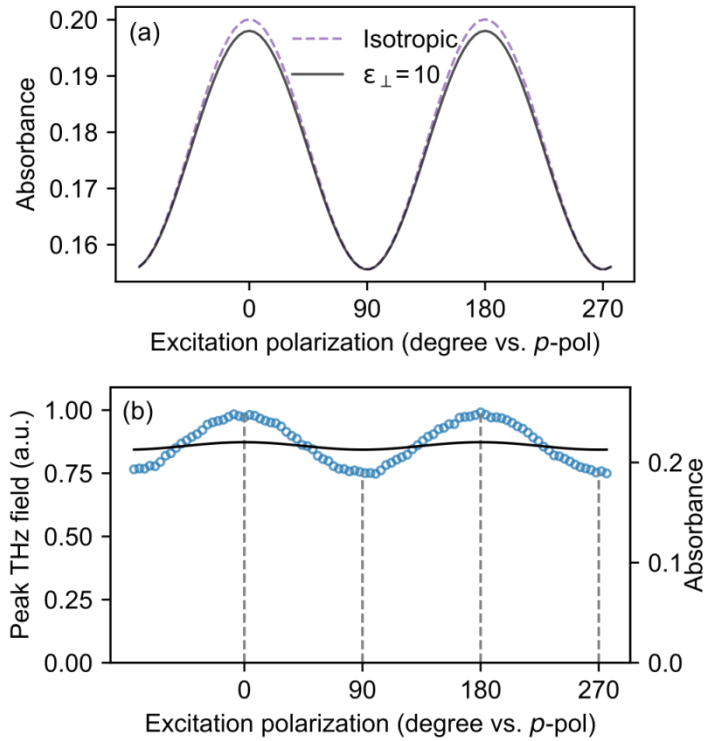


Fig. S5. Analysis of the optical properties calculation. (a) Dependence of the calculated absorption of WS₂/MoS₂ heterostructures on the out-of-plane dielectric function of the monolayers. The isotropic response corresponds to the scenario in which the out-of-plane permittivity is the same as the in-plane values. (b) Best-fit absorption calculation (solid black line) assuming a fused quartz substrate instead of the experimentally used sapphire substrate. The clear deviation from data (blue circles) here highlights the agreement in Fig. 2B.

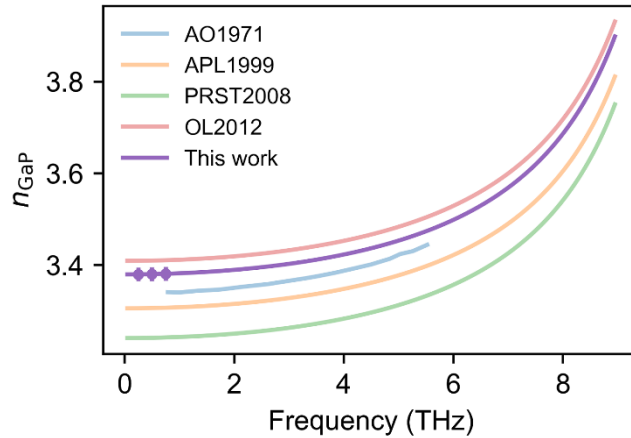


Fig. S6. Determination of THz refractive index of GaP. We noticed sizable differences between previously reported values of THz refractive index of GaP, likely due to variations in defect/dopant density. More specifically, the different reports have similar frequency dependence, but small offsets in absolute values. To be as quantitative as possible, we measured the low-THz refractive index of our 258- μm -thick GaP crystal with an interdigitated GaAs emitter (purple data points), and extrapolated the values in the experimentally relevant regime.

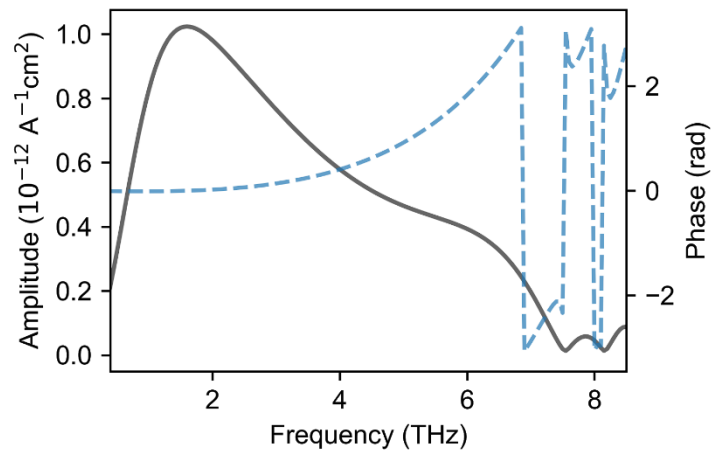


Fig. S7. Total transfer function of the setup. Amplitude (black solid line, left axis) and phase (blue dashed line, right axis) of the total transfer function that converts J_z to $\Delta I/I_0$ for the high-bandwidth setup in Fig. 3. The suppression at low frequencies is due to the finite NA of the collection optics and that at high frequencies due to limitations of the GaP EO crystal.

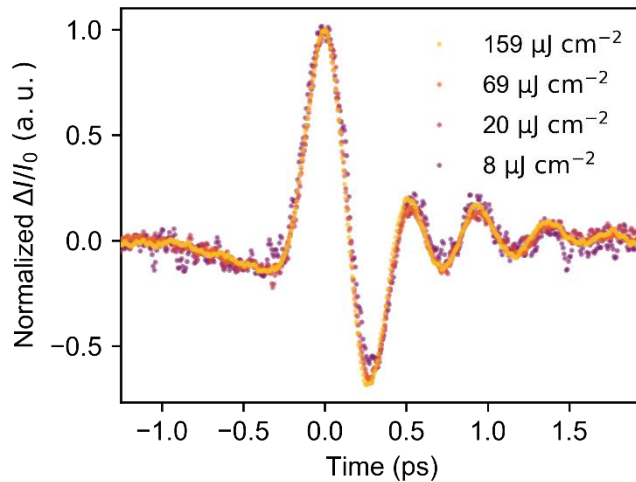


Fig. S8. Normalized THz waveforms for representative excitation fluences.

Normalized THz waveforms for representative excitation fluences in Fig. 4. The peak THz field remains a good measure of the interfacial current amplitude up to the highest fluence, since the normalized waveform is unchanged to experimental accuracy.

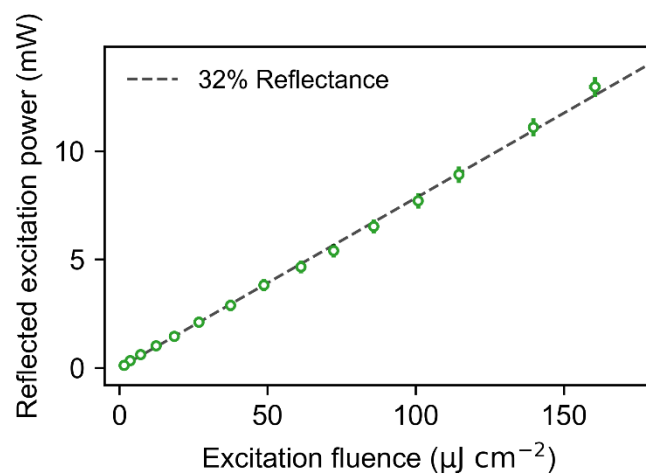


Fig. S9. Reflected excitation power as a function of excitation fluence. Reflected excitation power as a function of excitation fluence for the same condition as in Fig. 4. The dashed line is a linear fit for a reflectance of 32%. Note that the axes have different units. The constant reflectivity demonstrates that the absorption of the excitation energy has not saturated up to the highest fluence.